Applied Surface Science 258 (2012) 6884–6890

Contents lists available at SciVerse ScienceDirect

Applied Surface Science

journal homepage: www.elsevier.com/locate/apsusc

Magnetic property and corrosion resistance of electrodeposited nanocrystalline iron–nickel alloys

G.P. Pavithra, A. Chitharanjan Hegde*

Electrochemistry Research Laboratory, Department of Chemistry, National Institute of Technology Karnataka, Srinivasnagar 575 025, India

ARTICLE INFO

Article history:
Received 3 August 2011
Received in revised form 6 February 2012
Accepted 23 March 2012
Available online 30 March 2012

Keywords:
Nanocrystalline Fe–Ni alloy deposition
SEM
XRD
Magnetic property
Corrosion behavior

ABSTRACT

In the present investigation we have galvanostatically synthesized nanocrystalline Fe–Ni alloys on copper substrate. The effect of current density (c.d.) on composition, surface morphology and phase structure were studied for explaining the magnetic and electrochemical properties of the nanocrystalline alloy. The bath found to exhibit the preferential deposition of less noble Fe than Ni, and at no conditions of c.d., the deposition has changed from anomalous to normal type. Surface morphology and structural characteristics of the deposits were examined using scanning electron microscopy (SEM) and X-ray diffraction (XRD) analysis. As composition of the alloy varied, consequent to the current density a change of body centered cubic structure (bcc) to face centered cubic structure (fcc) was observed for nanocrystalline materials. Finally, the conditions responsible for peak magnetic property and corrosion resistance were optimized. Factors responsible for improved functional properties were explained in terms of surface morphology and crystalline grain size of the coatings.

1. Introduction

Development of new materials; and understanding of phase structures and surface morphology is at the root of progress of material science. This is particularly true in the development of new magnetic materials for a variety of important applications. In this regard, process of co-deposition of iron–nickel (Fe–Ni) alloys by electrochemical reduction in aqueous solutions has long been a subject of scientific and technological interest with the earliest studies dating back to the beginning of last century [1]. The solid state properties of these alloys which received considerable attention are their magnetic properties, and excellent corrosion resistance. They are used primarily as soft magnetic materials in the area of high-speed random-access computer memories [2]. This application region is dominated by perm-alloy type alloys, frequently with additional alloying elements. The relationships among the plating variables of Fe–Ni alloys are complicated by the nature of the co-deposition which is prevailing in mutual alloys of Fe-group metals.

The binary alloys of iron group metals, namely Fe–Ni, Fe–Co and Ni–Co electrodeposition exhibits peculiar phenomenon of 'anomalous co-deposition'. This term introduced by Brenner is being used to describe the preferential deposition of the less noble metal, Fe to the more noble metal, Ni [3]. In other words, the reduction of Ni is inhibited while the deposition of iron is enhanced when compared to their individual deposition rates. Hence, electrodeposition of Fe–Ni alloys has attracted considerable attention due to their special characteristic nature and wide range of unique properties.

Recently the phase structures of alloys have been analyzed by electrochemical techniques, such as galvanostatic and potentiostatic methods, and more often by anodic linear sweep voltammetry [4]. The literature pertaining to electrodeposition of mutual alloys of Fe group metals, namely Ni, Fe, Co and Zn, is rather exhaustive and many serious research works have been reported [4–8]. It has been identified that both face centered cubic (fcc) and body centered cubic (bcc) iron group metal alloy solid solutions have been produced by electrodeposition. These alloys were found to exhibit many useful properties such as high internal strength, hardness, high corrosion resistance and unusual magnetic properties. Many magnetic alloys with different compositions were widely employed for various purposes. Ferromagnetic alloys, e.g., Fe–Co and Fe–Ni are few among many, and have received considerable attention for their practical applicability in modern industries, such as in rockets, computers, space technology, etc. However, data on magnetic properties and corrosion resistance of electroplated Fe–Ni alloys are difficult to correlate as the wide variety of plating baths and their operating conditions used, and it is difficult to distinguish between the factors that significantly affect them [9,10]. There exists a complex relation between plating variables, like bath composition and operating parameters, and deposit characters, such as magnetic and corrosion properties due to peculiar anomalous co-deposition. Therefore, it is hard to develop Fe–Ni

* Corresponding author. Tel.: +91 9980360242; fax: +91 824 2474033.
E-mail address: acrhegde@gmail.com (A.C. Hegde).

0169-4332/$ – see front matter © 2012 Elsevier B.V. All rights reserved.
http://dx.doi.org/10.1016/j.apsusc.2012.03.124

Table 1
The bath composition (in gL^{-1}) and operating parameters of the optimized Fe–Ni bath.

Bath ingredients	Composition gL^{-1}	Operating parameters
$FeSO_4{\cdot}7H_2O$	16	c.d: 1.0–8.0 A dm^{-2}
$NiSO_4{\cdot}6H_2O$	100	pH: 3.5
H_3BO_3	30	Temperature: 303 K
L-Ascorbic acid, $C_6H_8O_6$	8.0	
Sulphanilic acid, $C_6H_7NO_3S$	1.0	

coatings of desired properties from aqueous electrolyte. In other words, magnetic properties and corrosion behavior of Fe–Ni alloy deposited from each bath is unique, in terms of the bath composition and operating parameters.

This paper presents the experimental study of electrodeposition of Fe–Ni alloys from sulphate bath on copper, combined with analyzing their structures, magnetic properties and corrosion potential. The effect of c.d. on composition, phase structure and morphology of the deposits were studied with particular emphasis on their magnetic property and corrosion behaviors.

2. Materials and methods

Plating solutions were prepared from reagent grade chemicals and distilled water. All depositions were carried out at 303 K. Commercial copper sheets of 50 mm × 20 mm × 2 mm were used as substrates (cathode), and pure nickel plate of same dimension used as anode. Copper panels having an exposed area of 7.5 cm^2 were used, with same exposed anodic area. The copper substrates were polished mechanically and then cleaned electrochemically. An acid sulfate solution was used as the electrolyte for deposition of Fe–Ni films. Bath composition and operating parameters are shown in Table 1. While ascorbic acid (AA) was used as antioxidant (to avoid anodic oxidation of Fe^{2+} to Fe^{3+}), sulphanilic acid (SA) was used as additive for brightening purpose. The optimal bath composition and operating parameters have been arrived by standard Hull cell method, described elsewhere [11].

Copper specimens after pre-cleaning were washed with distilled water and then immersed in the bath solution for electrolysis. All depositions were carried out for 10 min for comparison purpose. Thin Fe–Ni coatings were developed from the optimized bath, taken in 250 cm^3 PVC cell keeping the anode and cathode parallel at 5 cm distance. Electroplating was carried out at constant c.d.'s, viz. 1.0, 2.0, 4.0, 6.0, 8.0 A dm^{-2} using DC power source. (N 6705A, Agilent Technologies, USA). The pH of bath solution before and after every deposition was measured, and the change of pH was recorded (μ pH System-362, Systronics). Solution pH was adjusted to 3.0, using H_2SO_4 or NaOH. The copper panel, after deposition was rinsed with distilled water, and then air dried. The thickness of each coating was calculated from the weight of deposit, using Faraday's law. The hardness of the deposit was measured by Vickers method using micro-hardness meter (CLEMEX).

Magnetic properties of the Fe–Ni films were measured by a vibrating sample magnetometer (VSM) (ADE-DMS, EV-7). The VSM was calibrated using the standard calibration sample of nickel with 99.99% purity. The calibration was done at an applied magnetic field of 15,000 Oe, and a temperature of 20 °C. Hysteresis loops were generated using a sweep time of 20 min and a maximum field of 15,000 Oe. The dimensions of the Fe–Ni coating samples used in the VSM measurements were 5 mm × 5 mm. The corrosion behaviors of coatings were evaluated in 1 M KOH, by potentiodynamic polarization and electrochemical impedance spectroscopy (EIS) techniques (Potentiostat/Galvanostat, VersaSTAT3, Princeton Applied Research), keeping open to air and at room temperature. A three-electrode set-up described elsewhere [12] was used for corrosion study. A saturated calomel electrode (SCE) was used as the reference electrode. Polarization study was carried out in a potential ramp of ±250 mV from open circuit potential (OCP) at scan rate of 1 mV s^{-1}. EIS signals were recorded using AC signal of 10 mV amplitude, at a frequency range from 10 mHz–100 kHz. Surface morphologies and compositions of the Fe–Ni alloy coatings were examined by scanning electron microscopy (SEM), with energy dispersive X-ray (EDX) analyzer facility (JSM-6380 LA from JEOL, Japan). The phase structures of the coatings and their grain size were identified with X-ray diffractometer (XRD) (JEOL JDX-8P), using Cu Kα (λ = 1.5406 Å) radiation in continuous scan mode at scan rate of 2° min^{-1}. The grain size was evaluated using Scherrer formula shown in following equation.

$$D = \frac{K\lambda}{\beta \cos\theta} \quad (1)$$

where D is crystalline size, K is constant, λ is incident wavelength, β is full width at half maximum intensity and θ is Braggs angle.

3. Results and discussion

3.1. Alloy composition

Optimal composition and operating parameters of the proposed bath was arrived by Hull cell method. Variety of Fe–Ni coatings, having different composition formed on Hull cell panel indicated that c.d. plays an important role in the plating process. While overcoming the practical difficulties in developing a stable electrolytic bath for deposition of binary magnetic Fe–Ni alloy on copper, boric acid (BA) and ascorbic acid (AA) were used. A drastic change in pH of the electrolytic bath was found after plating. Hence, BA was used as buffer; prevented the drastic increase in pH of the bath after each deposition. A chemically stable bath was achieved by adding AA, an antioxidant to prevent oxidation of Fe^{+2} into Fe^{+3} ions. Sulphanilic acid (SA) was used as brightener, to impart mirror finish to the coating. The optimal bath constituents and operating parameters, after Hull cell optimization is given in Table 1. The deposit over the wide c.d. range of the Hull cell panel was found to be bright, i.e., in the range of 1.0–8.0 A dm^{-2}. Hence Fe–Ni alloys, having varied compositions were developed from the optimized bath at different current densities, keeping anode and cathode parallel to each other. The effect of c.d. on wt.% of Ni, hardness, and crystallite grain size of the coatings are discussed in the following sections.

3.1.1. Effect of c.d. on wt.% of Ni

The composition of electroplated Fe–Ni alloys may be described by the percentage of one alloy component, e.g., nickel, is plotted against the relative percentage of the respective metal ions, i.e., Ni^{+2} in the plating bath [2]. It should be noted that in the present Fe–Ni alloy bath, as given in Table 1, the wt.% of Ni and Fe in the bath are found to be respectively, 89% and 11%. Neglecting a small deviation, an increase of Ni wt.% in the deposit with increasing applied c.d. was observed. This is supported by the deposition principle of mutual alloys of Fe-group metals that an increase in the c.d. or temperature results in an increase of more noble metal in the deposit [13].

The variation in the wt.% of Ni in the deposit with c.d., shown in Fig. 1, revealed that under no conditions of c.d., wt.% Ni in the deposit has not reached the bath composition, i.e., the wt.% Ni in the deposit was found to be always less than that in the bath. Hence it may be inferred that, the bath follows anomalous deposition of Fe^{+2} and Ni^{+2} ions at all conditions of c.d. employed in this study.

Further, it was observed that at c.d. larger than 2.0 A dm^{-2}, the wt.% of Ni in the deposit was found to increase with c.d. At 4.0 A dm^{-2}, the bath produced a sound and bright deposit having ~81.5 wt.% of Ni. This increase in Ni wt.% with c.d. (Fig. 1) indicates that the deposition process is tending towards normal type. But at low c.d. (< 2.0 A dm^{-2}) the bath exhibited the opposite trend, i.e.,

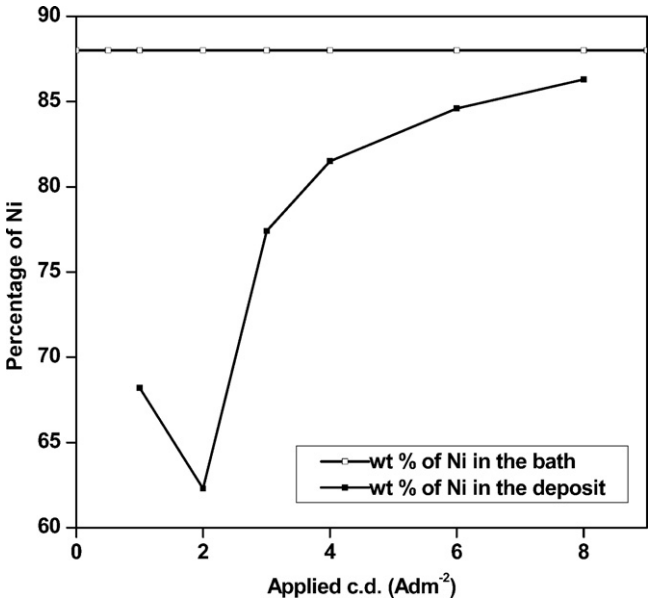

Fig. 1. Variation in wt.% Ni in the deposit with applied c.d., deposited from optimal Fe–Ni bath at 303 K and pH 3.0.

it decreased with increase of c.d., as shown in Fig. 1. This is due to the tendency of bath to co-deposit in anomalous fashion than normal type, as envisaged by Brenner [3]. This observation at low c.d. and elevated temperature are characteristic of all mutual alloys of Fe-group metals due to significant mass transport effects during deposition.

3.2. Surface morphology

The effect of c.d. on surface morphology of Fe–Ni coatings was studied by electron microscopy. The microstructure of the coatings at different c.d.'s is shown in Fig. 2. It should be noted that the surface morphology of electroplated Fe–Ni coating is greatly influenced by c.d. employed. Sanaty et al. observed that increasing the iron content in the deposit decreases the grain size [14]. Generally, crystallization occurs either by the buildup of old crystals, or by the formation and growth of new ones. These two processes are in competition and can be influenced by different factors. Low surface diffusion rates, high population of adatoms and high overpotentials are factors responsible for creation of new nuclei [15]. At low c.d. the deposit was found to be very smooth and uniform as shown in Fig. 2(a).

It is clearly observed from Fig. 2 that as c.d. increased the grain size also increased. At very high c.d. ($8.0\,A\,dm^{-2}$) the deposit was found to be very porous, with globular structure. It may be due to high wt.% of nobler Ni in the deposit, caused by reduced inhibitory action of hydroxyl ions.

3.3. Phase structure

The crystal orientation of electrodeposited Fe–Ni alloys with different compositions can be characterized by means of XRD analysis. The identification of the phases of the deposits was obtained from the peak profiles of the X-ray reflection plotted as a function of 2θ as shown in Fig. 3. It was observed that the deposits were in

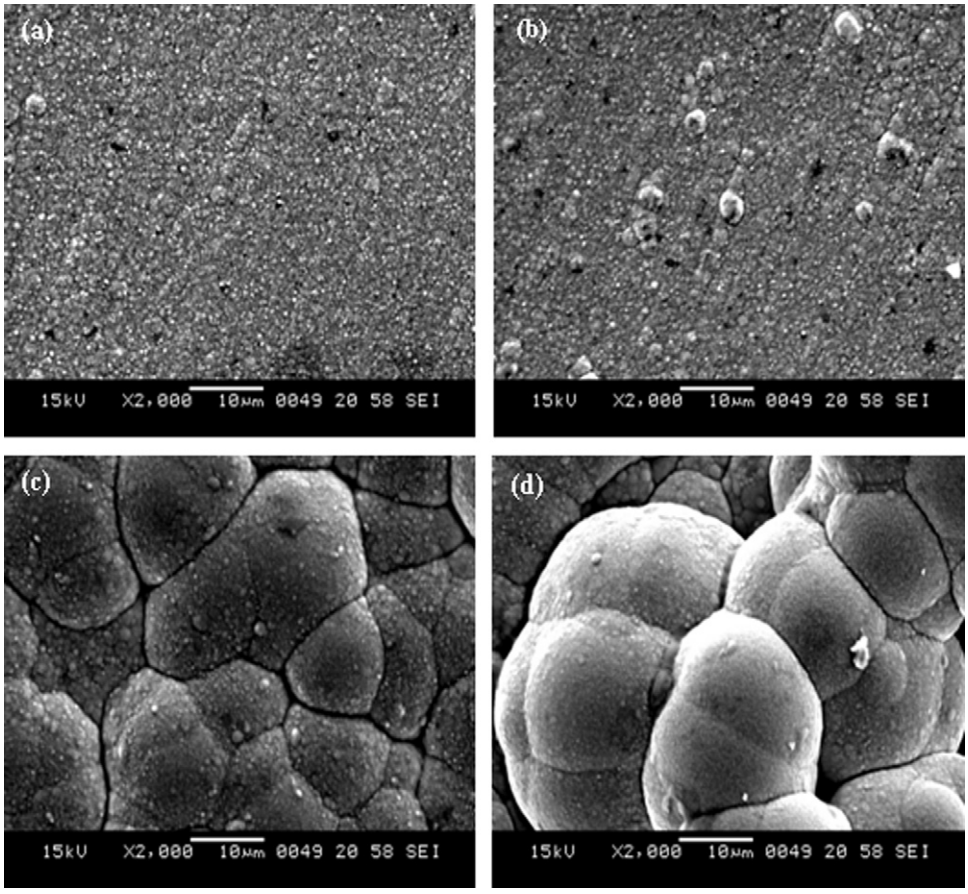

Fig. 2. SEM micrographs Fe–Ni coatings deposited from optimized bath at (a) $2.0\,A\,dm^{-2}$, (b) $4.0\,A\,dm^{-2}$, (c) $6.0\,A\,dm^{-2}$, (d) $8.0\,A\,dm^{-2}$.

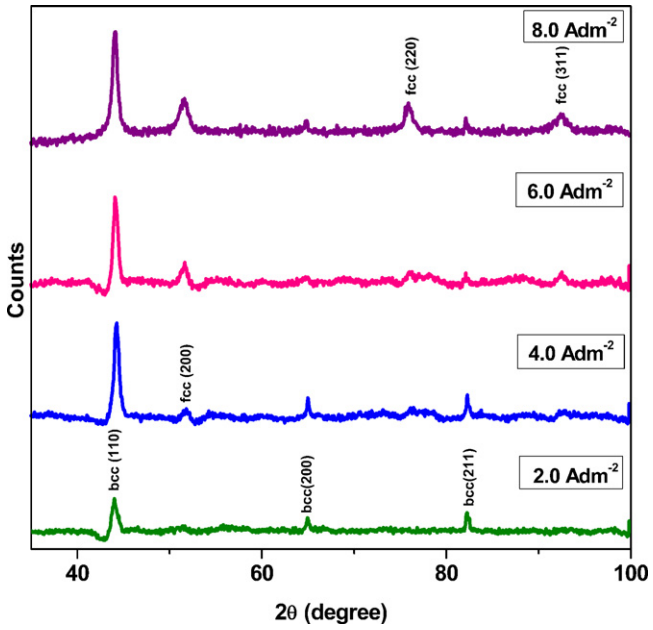

Fig. 3. X-ray diffraction patterns of Fe–Ni alloys electrodeposited from the optimized bath at different c.d.'s.

nanometric range (2–10 nm), their size slightly increasing with an increase in applied c.d.

XRD signals of Fe–Ni coating at 2.0 A dm^{-2} showed single phase bcc related to Fe crystal structure. As cathode c.d. increased, the wt.% of Ni in the deposit increased. Accordingly an increase in fcc phase structures corresponding to increased Ni content was observed. At 4.0 A dm^{-2}, the alloy consisting of both bcc and fcc crystal structures was formed as is obvious in related pattern. Since the Ni peak pattern coincides with the peak pattern of $FeNi_3$, the existence of $FeNi_3$ inter-metallic is quite likely. This is further supported by a recent study on nanocrystalline Ni–Fe alloy [16]. Accordingly there exists a larger probability of formation of an ordered $FeNi_3$ intermetallic structure due to faster grain boundary diffusion.

To know the preferred orientation of the deposit in detail, the texture coefficient (T_C) value was employed. Based on the relative intensities of the bcc and fcc peaks, it is possible to find the T_C value of Fe–Ni electrodeposit using XRD data. The method developed by Be'rube' and L'Esperance has been used for calculating the value of T_C, and is given by following equation.

$$T_C(h\ k\ l) = \frac{I(h\,k\,l)}{I_0(h\,k\,l)} \times \frac{\sum I_0(h\,k\,l)}{\sum I(h\,k\,l)} \quad (2)$$

where $I(h\,k\,l)$ is the peak intensity of Fe–Ni electrodeposits and $\Sigma I(h\,k\,l)$ is the sum of intensity of all the diffraction peaks. The index 0 refers to the intensities of the peaks of standard Fe–Ni sample. If the T_C is greater than 1.0, it indicates the existence of preferred orientation. It may be noted that volume fraction of bcc is found to be higher than that of fcc at low c.d. As the c.d. increased fcc phase became predominant over the bcc phase in the deposit.

Fig. 4(a) and (b) shows the relationship between the applied c.d. and the T_C of bcc and fcc phases respectively. In the bcc phase, the T_C values for the (2 0 0) and (2 1 1) orientations were greater than unity. It indicates that the preferred orientation of the deposit at low c.d. is of dual texture, i.e., (2 0 0) and (2 1 1). However at 4.0 A dm^{-2}, (2 1 1) texture decreased and altogether disappeared at high c.d. On the other hand, in the fcc phase, (1 1 1) texture predominates. On increasing the c.d. further, the preferred orientation of the fcc phase changed sharply from (1 1 1) to (2 2 0). Thus from the XRD patterns and the T_C values, it may be concluded that at

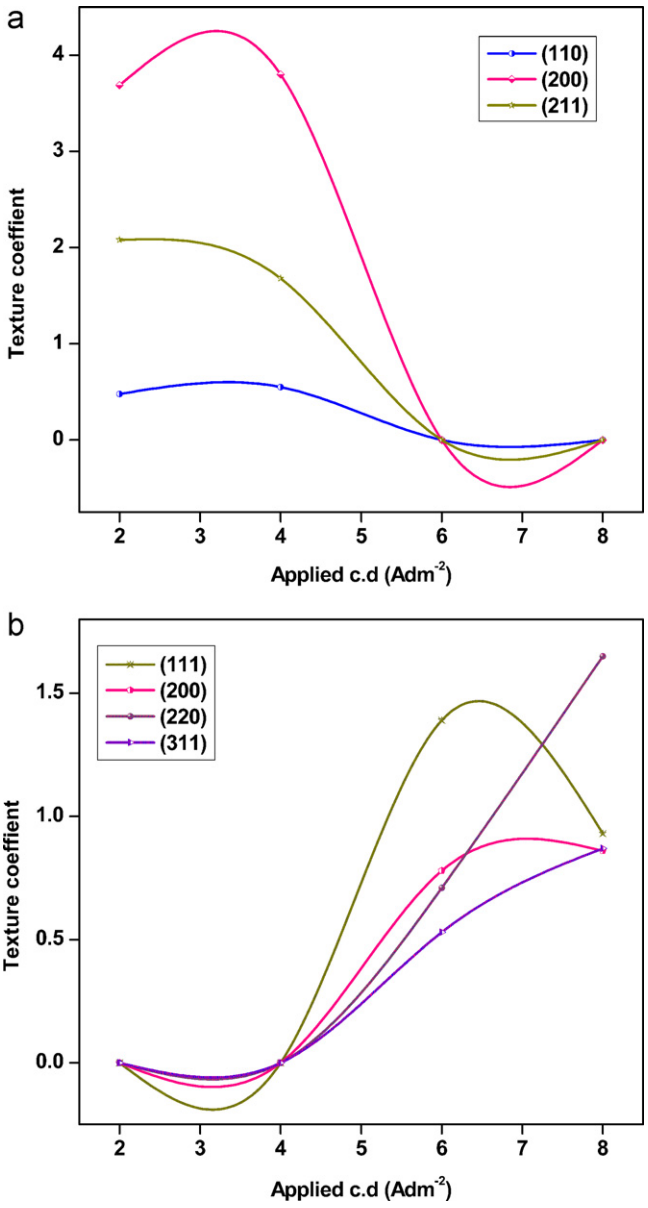

Fig. 4. Variation of texture coefficient, T_C of electrodeposited Ni–Fe alloy with applied c.d. of (a) bcc phase (b) fcc phase.

low c.d., the volume fraction of bcc is greater than that of fcc with predominance of (2 0 0) and (2 1 1) texture. Hence as c.d. increased, the volume fraction of fcc increased. Therefore fcc (2 2 0) texture developed strongly as shown in Fig. 4(b).

3.4. Micro hardness

The micro-hardness of the Fe–Ni alloy deposited from the proposed bath was found to increase with the c.d. employed for its deposition. As seen in Fig. 5, there was a slight decrease in hardness of the deposit with increasing Fe content. This is in contrast to the results reported in the literature [16], wherein an increase in Fe content led to an increased hardness. McCrea et al. observed a moderate decrease in hardness with increasing Fe content in the fcc range; and a significant increase with Fe content in the bcc range [17]. However, Cheung et al. showed that the hardness of Fe–Ni alloy increased with Fe content up to 16.5%, and then decreased [18]. Therefore at higher c.d., there exists a formation of intermetallic

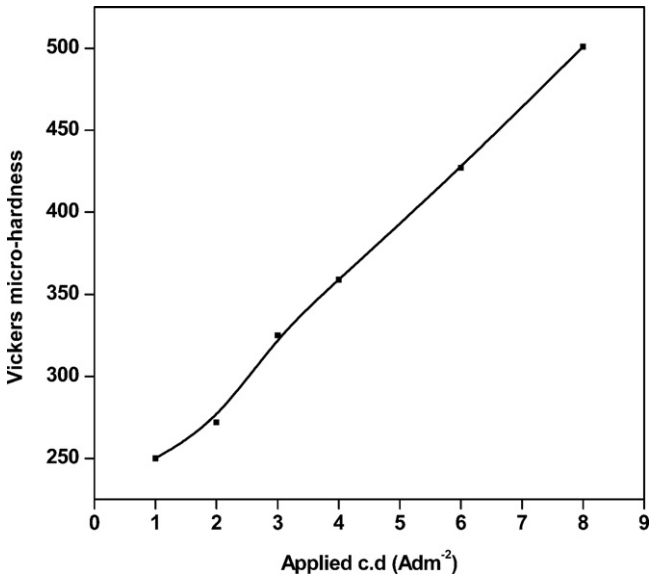

Fig. 5. Variation of micro-hardness of Fe–Ni coatings deposited with different applied c.d. from the optimized bath.

$FeNi_3$ phase, evidenced by XRD analysis and is responsible for the overall hardness of the electrodeposit.

3.5. Magnetic property

It is well known that the magnetic properties of the materials depend on the chemical composition and grain size [19]. The magnetic properties of Fe–Ni coated films were measured at room temperature using VSM. The hysteresis curve of Fe–Ni films are shown in Fig. 6. It was found that the Fe–Ni alloys exhibit ferromagnetic property, but no super-paramagnetic phenomenon was observed. The saturation magnetization, M_S and coercivity, H_c of Fe–Ni deposits at different c.d.'s are given in Table 2. The observed decrease of M_S, and an increase of H_c with deposition c.d. may be explained as follows.

Bulk Fe and bulk Ni are known to be ferromagnetic with M_S value equal to 220 emu g^{-1} and 55 emu g^{-1} respectively. The decrease of M_S with increase in c.d. is due to decrease of grain size from bulk to nano. It is known that M_S is dependent on the number of magnetic molecules in a single magnetic domain, and hence it is proportional to the size of the material [20].

Generally, the M_S value increases with Fe content in the deposit [8]. The attracting feature here is that with the increase in Fe content, the M_S value is found to decrease. This may be related to the decrease of grain size, associated with Fe content of the deposit. Moreover, the presence of $FeNi_3$ super lattice phase contributed to the magnetization [2].

Further, the coercivity value is found to decrease constantly with c.d. as reported in Table 2. Generally, a smaller grain size leads to an increase in coercivity [21]. In the present study, the coercivity can also be linked to the phase structure of the alloys. As seen in XRD study, phase transformation from bcc to fcc occurred with an increase in applied c.d. Tabakoviv and co-workers have found that materials with single bcc phase show high coercivity [22]. Here, at 2.0 A dm^{-2} c.d., bcc phase dominated leading to a high coercivity. As the c.d. increases to 4.0 A dm^{-2}, along with bcc phase the alloy exhibited a slight fcc phase. In other words, there was a formation of mixed phase which leads to reduction in coercivity. At higher c.d. there was a complete transition of bcc to fcc phase, and hence the coercivity decreased.

Table 2
Variation of saturation magnetization, M_s and coercivity, H_c of electrodeposited Fe–Ni alloy with applied c.d.

Applied c.d. (A dm^{-2})	M_s (emu g^{-1})	H_c (Oe)
2.0	3.51	17.60
4.0	6.16	15.95
6.0	8.13	15.00
8.0	9.50	14.00

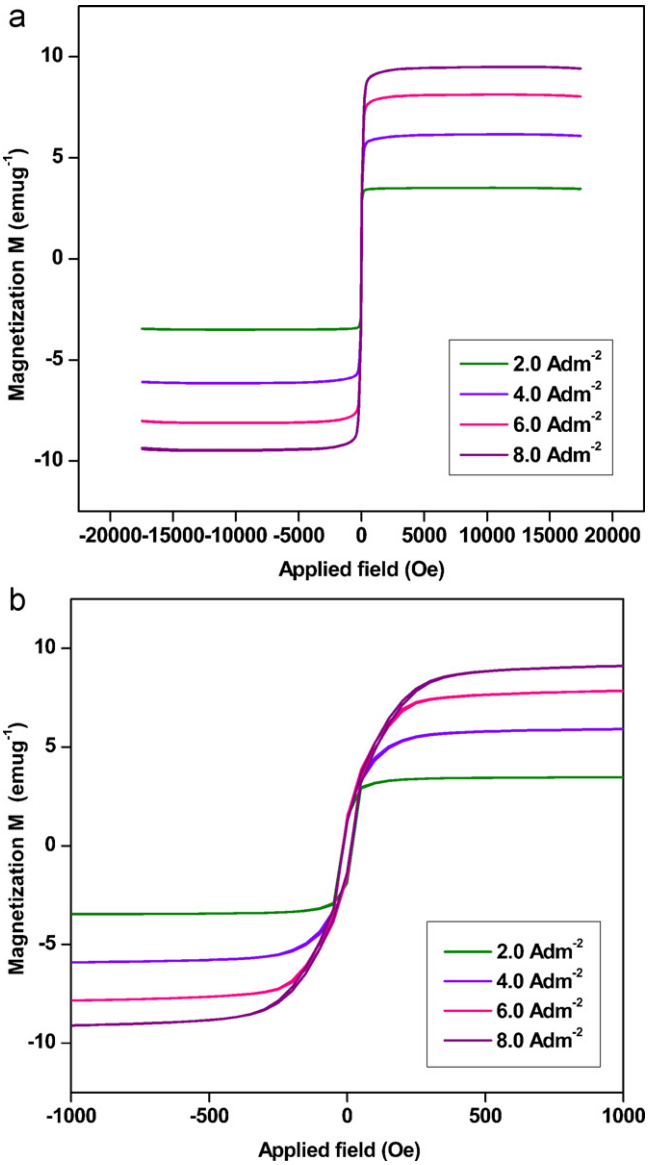

Fig. 6. (a) Magnetization curve of Ni–Fe coatings deposited at different applied c.d.'s (b) enlarged view at close proximity of applied magnetic field.

The variation of crystallite grain size and coercivity of the electrodeposited Fe–Ni alloy coatings with applied c.d.'s are shown in Fig. 7. It may be observed that crystallite grain size and coercivity show almost inverse dependence with each other over the range of applied c.d. studied, in compliance with discussion made earlier.

3.6. Potentiodynamic polarization study

The corrosion behaviors of electrodeposited Fe–Ni alloys have been evaluated by potentiodynamic polarization method. The corrosion rates were calculated by Tafel's extrapolation method. The

Table 3
Corrosion parameters of Fe–Ni alloy coating deposited from the optimized bath at different c.d.'s.

c.d. ($A\,dm^{-2}$)	E_{corr} (mV) vs. SCE	β_a ($V\,dec^{-1}$)	β_c ($V\,dec^{-1}$)	i_{corr} ($\mu A\,cm^{-2}$)	CR ($mm\,y^{-1}$)
2.0	966.3	0.031	0.025	102.6	1.1535
4.0	936.9	0.037	0.030	51.89	0.5830
6.0	1020.6	0.044	0.038	60.87	0.6839
8.0	795.2	0.230	0.240	65.25	0.7330
Cu	323.0	0.044	0.050	182.3	2.1275

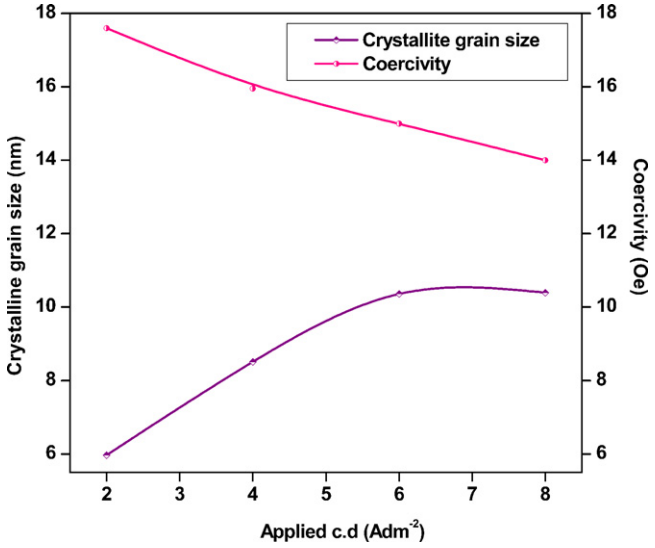

Fig. 7. Variation of crystalline grain size and coercivity of electrodeposited Fe–Ni alloy over range of applied c.d.

Tafel's behavior of Fe–Ni alloy coatings at different c.d., like 2.0, 4.0, 6.0 and 8.0 $A\,dm^{-2}$ is shown in Fig. 8, and corresponding corrosion data are reported in Table 3.

It should be noted that Fe–Ni alloys deposited at different c.d.'s are characterized by high E_{corr}, and the passivity regime begins at less negative potentials. Further, the corrosion rate (CR) decreased with an increase of c.d., as a function of change in the phase structure of the deposits. It is observed that Fe–Ni coating, at 4.0 $A\,dm^{-2}$ exhibits least CR (0.5830 $mm\,y^{-1}$) due to variation in phase structures.

The XRD signals corresponding to 4.0 $A\,dm^{-2}$ in Fig. 3 shows an intermittent transitional phase from bcc to fcc. During this transition, the Fe content tends to decrease and Ni content tends to increase. Ni being nobler compared to Fe, a decrease of corrosion rate was observed. But, further increase of c.d. resulted in decrease of CR as shown in Table 3. This is attributed to high porosity of the coatings, due to increase in Ni content and $FeNi_3$ phase. This is in compliance with surface morphology of the Fe–Ni coatings as shown in Fig. 2.

3.7. Electrochemical impedance spectroscopy

EIS was used to evaluate the barrier properties of the coatings. The nyquist plots of the coated samples deposited at different c.d. are shown in the Fig. 9. The Nyquist plots showed a single semicircle for all samples. At higher frequencies the interception of real axis is ascribed to the solution resistance (R_s) and at the lower frequencies, the interception with real axis is ascribed to the charge transfer resistance (R_{ct}). R_{ct} increases from 2Adm^{-2} to 4 $A\,dm^{-2}$ then decreases, which shows that the Fe–Ni alloy deposited at 4 $A\,dm^{-2}$ has good corrosion resistance.

Equivalent circuit for the monolithic Fe–Ni alloy is shown in Fig. 10. It consists of double layer capacitance (Q_{dl}), which is parallel to charge transfer resistance (R_{ct}); both of which are in parallel with coating capacitance (Q_{coat}) and charge transfer resistance for the porosity of the coating (R_{pore}). All these elements are in series with solution resistance (R_s) between the working electrode (WE) and the tip of the Luggin capillary. When the coated sample is immersed in the electrolyte, the corrosion is expected to initiate rapidly at the pores present in the coating because of low coating thickness. This leads to the formation of localized galvanic cells, which dominate

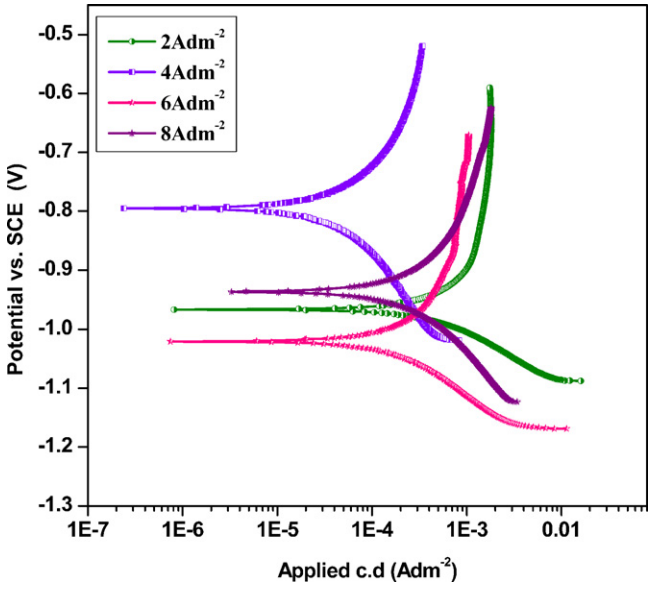

Fig. 8. Potentiodynamic polarization behavior of Fe–Ni coatings deposited from the optimal bath at different c.d.'s.

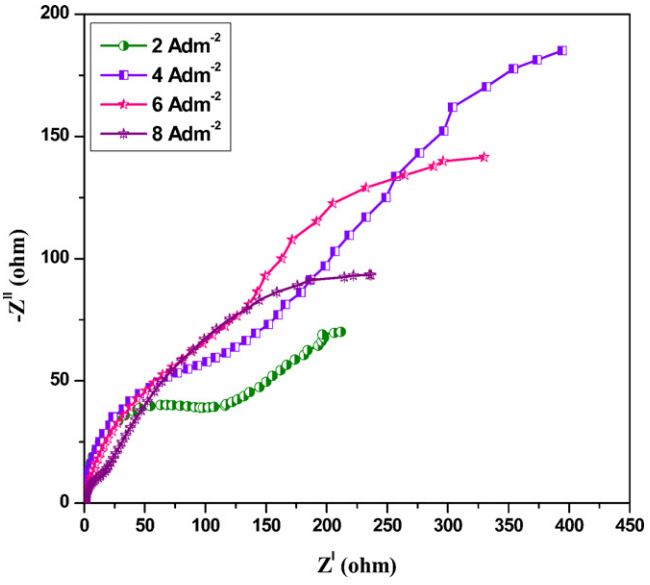

Fig. 9. Nyquist plots of Fe–Ni coatings deposited at varying c.d.

Table 4
EIS data obtained by equivalent circuit simulation of coatings deposited at varying c.d.

c.d. ($A\,dm^{-2}$)	R_s ($\Omega\,cm^2$)	Q_{coat}–Y_0 ($\mu F\,cm^{-2}$)	n_c	R_{pore} ($\Omega\,cm^2$)	Q_{dl}–Y_0 ($\mu F\,cm^{-2}$)	n_{dl}	R_{ct} ($\Omega\,cm^2$)
2	0.3594	35.59	1.0	87.11	69	0.8	299.0
4	0.2793	40.85	1.0	197.30	25	0.5	1919.0
6	0.4278	67.79	0.9	71.60	21	0.4	830.2
8	0.4591	88.80	1.0	11.82	10	0.5	408.8

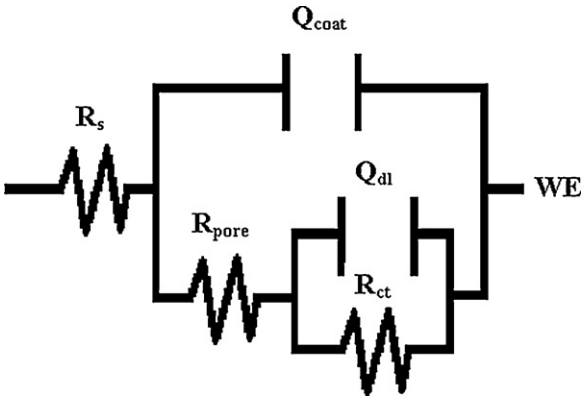

Fig. 10. Equivalent circuit used for fitting the electrochemical impedance data of Fe–Ni alloy.

the galvanic corrosion process. In such cases, electrochemical interface can be divided into two sub-interfaces-electrolyte/coating and electrolyte/substrate. From EIS data given in Table 4, it is seen that Q_{coat} decreased for the Fe–Ni coating deposited at $4.0\,A\,dm^{-2}$, this represents less defective nature of the coatings. Hence they show good corrosion resistance.

4. Conclusions

A sulphanilic acid sulphate bath has been proposed for galvanostatic deposition of bright Fe–Ni alloy on copper substrate and following conclusions are drawn:

1. The bath exhibited codeposition of anomalous type at all c.d.'s studied, and cathode c.d. is found to determine the deposition of alloys of different composition, having different phase structures.
2. XRD study of electrodeposited alloys revealed that volume fraction of bcc structure is higher than that of fcc at low c.d.; and as c.d. increased, fcc phase becomes predominant over the bcc phase.
3. At higher c.d., an intermetallic phase, $FeNi_3$ was observed with increased grain size. The micro-hardness of the deposits was found to increase with c.d. as a function of phase structures.
4. Saturation magnetization M_s increased and coercivity, H_c of Fe–Ni coatings decreased over the c.d. range studied, and are associated with the changed crystallite grain size and phase structure.
5. Corrosion study demonstrated that at $4.0\,A\,dm^{-2}$, the bath produces the least corrosive Fe–Ni coating ($CR = 0.5830\,mm\,y^{-1}$) having about 81.5% of Ni compared to the coatings at other c.d.'s. Further, the XRD study revealed that at this c.d., phase structure of alloy changed from bcc to fcc pattern.
6. From impedance datas, obtained from the EIS measurements showed the values of the charge transfer resistance and the pore resistance showed gradual increase from deposited c.d. $2.0\,A\,dm^{-2}$ to $4.0\,A\,dm^{-2}$ and then decreases. For all the coated samples, the coating capacitance and double layer capacitance shows small variations, indicating that the surface of the coated substrate was less affected.

Acknowledgement

Author is grateful to NITK, Surathkal, for providing the Institute fellowship for carrying out this work.

References

[1] M. Matlosz, Competitive adsorption effects in the electrodeposition of iron–nickel alloys, J. Electrochem. Soc. 140 (1993) 2272–2279.
[2] R. Štefec, Magnetic properties of electrodeposited iron–nickel alloys, Czech. J. Phys. B 23 (1973) 1249–1260.
[3] A. Brenner, Electrodeposition of Alloys – Principles and Practice, vols. 1 and 2, Academic Press, 1967.
[4] A.R. Despic, V.D. Jovic, in: R.E. White, J.O'M Bockris, B.E. Conway (Eds.), Modern Aspects of Electrochemistry, Plenum Press, New York, 1995.
[5] L. Ricq, F. Lallemand, M.P. Gigandet, J. Pagetti, Influence of sodium saccharin on the electrodeposition and characterization of CoFe magnetic film, Surf. Coat. Technol. 138 (2001) 278–283.
[6] R. Fábio Bento, L.H. Mascaro, Analysis of the initial stages of electrocrystallization of Fe, Co, and Fe–Co alloys in chloride solutions, J. Braz. Chem. Soc. 13 (2002) 502–509.
[7] E. Jartych, M. Jalochowski, M. Budzynski, Influence of the electrodeposition parameters on surface morphology and local magnetic properties of thin iron layers, Appl. Surf. Sci. 193 (2002) 210–216.
[8] N.V. Myung, K. Nobe, Electrodeposited iron group thin-film alloys, structure–property relationships, J. Electrochem. Soc. 148 (2001) 136–144.
[9] S.D. Leith, Shirley Ramli, Daniel T. Schwartz, Characterization of Ni_xFe_{1-x} ($0.10 < x < 0.95$) electrodeposition from a family of sulfamate–chloride electrolytes, J. Electrochem. Soc. 146 (1999) 1431–1435.
[10] J.O'.M. Bockris, A.K.N. Reddy, M.G. Aldeco, Modern Electrochemistry, Kluwer Academic, Plenum Publishers, 2000.
[11] N. Kanani, Electroplating: Basic Principles, Processes and Practice, Elsevier Ltd, Berlin, Germany, 2006.
[12] D.A. Jones, Principles and Prevention of Corrosion, Prentice Hall, New York, 1996.
[13] H. Schultz, M. Pritzker, Modeling the galvanostatic pulse and pulse reverse plating of nickel–iron alloys on a rotating disk electrode, J. Electrochem. Soc. 145 (1998) 2033–2042.
[14] A. Saanaty-Zadeh, K. Raessi, A. Saidi, Properties of nanocrystalline iron–nickel alloys fabricated by galvanostatic electrodeposition, J. Alloys Compd. 485 (2009) 402–407.
[15] F. Ebrahim, H.Q. Li, Structure and properties of electrodeposited nanocrystalline FCC Ni–Fe alloy, Rev. Adv. Mater. Sci. 5 (2003) 134–138.
[16] H.Q. Li, F. Ebrahimi, Synthesis and characterization of electrodeposited nanocrystalline nickel–iron alloys, Mater. Sci. Eng. A 347 (2003) 93–101.
[17] J.L. McCrea, G. Palumbo, G.D. Hibbard, U. Erb, Properties and applications for electrodeposited nanocrystalline Ni–Fe alloys, Rev. Adv. Mater. Sci. 5 (2003) 252–258.
[18] C. Cheung, F. Djuanda, U. Erb, G. Palumbo, Electrodeposition of nanocrystalline Ni–Fe alloys, Nano-Struct. Mater. 5 (1995) 513–523.
[19] C. Suryanarayana, Nanocrystalline materials, Int. Mater. Rev. 40 (1995) 41–64.
[20] S.-H. Wu, D.-H. Chen, Synthesis and characterization of nickel nanoparticles by hydrazine reduction in ethylene glycol, J. Colloid Interface Sci. 259 (2003) 282–286.
[21] Yin Liu, Xia-ying Qin, Tai Qiu, Magnetic properties of nanostructural y-Ni–28Fe alloy, Trans. Nonferrous Met. Soc. China 16 (2006) 1370–1373.
[22] I. Tabakovic, S. Riemer, V. Inturi, P. Jallen, A. Thayer, Organic additives in the electrochemical preparation of soft magnetic CoNiFe films, J. Electrochem. Soc. 147 (2000) 219–226.